11. ISEORGANISEERITUS

11.1 Sissejuhatus

Tänapäeva intrigeerivaim modelleerimisülesanne
- pole seotud ainult matemaatiliste mudelite koostamine ja lahendamisega;
- nõuab tunnetusliku külje läbitöötamist.

Ilya Prigogine – Nobel 1977
Brüssel, dissipatiivsed struktuurid

Herman Haken – Stuttgart, sünergeetika

sünergeetika – avatud süsteemide teooria

dissipatiivsed

struktuurid – tasakaalust eemal tekkinud struktuurid;
"dissipatiivsed" – märgib dissipatiivsete protsesside osa
ka: hajusstruktuurid

Analüüs põhineb termodünaamikal

Mõisted:

entroopia = oleku muutuja S, mis määrab süsteemi oleku

q – soojusvoog

T – temperatuur

$dS > \frac{q}{T}$ entroopia saab ainult kasvada

$dS = \frac{q}{T}$ pööratava oleku jaoks

Statistiline termodünaamika

entroopia on mikroolekute arvu mõõt

informatsiooniteooria:

entroopia on informatsiooni mõõt

Seadused:

0. formaliseerib temperatuuri T
1. määrab siseenergia
2. määrab entroopia kasvu
3. määrab entroopia ja siseenergia kui absoluutne temperatuur läheneb nullile

Süsteemid:

avatud - massi, soojuse ja töö vahetus

suletud - soojuse ja töö vahetus massi ei vahetata

isoleeritud - mingit vahetust ei toimu

Temperatuur:

soojusvoo mõõt

nullpunkt $(^{\circ}K)$ - ei anna mingit soojust

madalaim teada olev $9 \cdot 10^{-8}\,\mathrm{K}$

kõrgem (Maal) $\sim 10^{7}\,\mathrm{K}$

11.2 Termodünaamilised süsteemid

Süsteemide kolm arengufaasi:

1. Tasakaal

$$\left.\begin{array}{l}\text{entroopia toodang}\\ \text{vood}\\ \text{jõud}\end{array}\right\} = 0$$

2. Tasakaalu ümbrus

   termodünaamilised "jõud" on nõrgad muutused väljendatud <u>lineaarsete</u> funktsioonidena

3. Kaugel tasakaalust

   muutused <u>mittelineaarsed</u>

P isoleeritud süsteem

Väljaspool tasakaalu

P ↔ R R reservuaar millel fikseeritud temperatuur T

Näide

Päike	Maa	Universum
R_1	P	R_2
lõpmatu reservuaar T_1	lõplik energia voog	lõpmatu reservuaar T_2

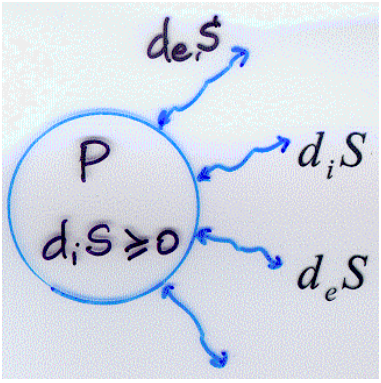

– entroopia toodang süsteemis
i - internal

– entroopia juurdevoog
e –external

1. Tasakaal

Elastsusteooria on termodünaamiliselt tasakaalus

$$d_i S = 0$$

2. Tasakaalu ümbrus
lineaarne termodünaamika

2.1 Vastastikuse mõju seadused (reciprocity)

Jõud “1” (temperatuuri gradient) mõjutab
voogu “2” (difusioon)

Jõud “2” (kontsentratsiooni gradient) mõjutab
voogu “1” (soojusvoog)

2.2 Süsteem pürgib tasakaalu poole, miinimum
entroopia kasv

→ stabiilne, determineeritud käitumine

3. Mittelineaarne termodünaamika

Olekute stabiilsus?

Tasakaalu olekute arv?

Fluktuatsioonid? Kuidas? Miks?

→ uus dünaamiline olek
dissipatiivne struktuur (hajusstruktuur)

11.3 Formalism

Olgu süsteem P ja reservuaarid R_j

Hamiltoniaan:

$$H = T + U$$

kineetiline energiad — potentsiaalne

$H = H(q,p)$ q - üldistatud koordinaat

p - üldistatud kiirus

$$p = \frac{\partial L}{\partial \dot{q}_j}, \qquad L = T - U$$

$$H = H_P + H_{R_1} + H_{R_2} + \ldots + H_{PR_1} + H_{PR_2} + \ldots$$

süsteem — reservuaarid — seostatus

Klassikaline (analüütiline) mehaanika

$$\dot{p}_j = -\frac{\partial H}{\partial q_j}$$ (vt. loeng 6)

$$\dot{q}_j = \frac{\partial H}{\partial p_j}$$

meetodid lihtsustamiseks,

reservuaaride mõju viimine ühtsetele muutujatele

Lõpptulemus:

$$\dot{q}_j = -\frac{\partial H}{\partial q_j} +$$ sumbuvus + fluktuatsioonid

$$\vec{q} = \{ q_j \}, \quad j = 1, 2, ..., n$$

n – võib olla väga suur

Esialgne hinnang – tasakaalu ümber, $\vec{q}_0$

$$\vec{q} = \vec{q}_0 + \vec{w}(\vec{X}, t)$$

$$\dot{\vec{q}} = M(...) \rightarrow \dot{\vec{w}} = L(\vec{q}_0)\,\vec{w}$$

lineaarne

Lineaarse võrrandi lahend

$$\vec{w}(\vec{X}, t) = e^{\lambda t}\, v(\vec{X})$$

$\mathrm{Re}\lambda > 0$ lahend kasvab $\exp(\lambda_u t) v_u(\vec{X})$

$\mathrm{Re}\lambda < 0$ lahend kahaneb $\exp(\lambda_s t) v_s(\vec{X})$

$$\vec{q} = \vec{q}_0 + \sum_u \xi_u(t)\vec{v}_u + \sum_s \xi_s(t)\vec{v}_s$$

ξ_u, ξ_s - amplituudid

Asendades esialgsesse võrrandisse $\dot{\vec{q}} = M(...)$

Saame:

$$\dot{\xi}_u = \lambda_u \xi_u + M_u(\xi_u, \xi_s) + F_u(t)$$

$$\dot{\xi}_s = \lambda_s \xi_s + M_s(\xi_u, \xi_s) + F_s(t)$$

↑ fluktuatsioonid

Allutusprintsiip (slaving principle)

$$\xi_s = f_s(\xi_u(t), t)$$

vabadusastmete (võrrandite) arv väheneb oluliselt

$$\dot{\xi}_u = \lambda_u \xi_u + M_u'(\xi_u) + F_u(t)$$

ξ_u – makroskoopilise korra parameetrid (order parameters)

q_j	**kasutusala**
molekulide tihedus	keemilised reaktsioonid
kiirusväli	hüdrodünaamika
temperatuuri väli	faasimuutused (tardumine)
elektromagnetiline väli	plasmafüüsika
polarisatsioon	võnkumised
loomade arv	populatsioonidünaamika
rakkude arv	morfogenees
neuronite aktiivsuse mõõt	närvivõrgud
finantside voog	majandus

$$\dot{\vec{q}}\left(\vec{X},t\right)=M\left(\vec{q},\ \underset{\frac{\partial}{\partial X_1},\frac{\partial}{\partial X_2}}{\nabla},\ \int\ldots\underset{\text{integral ruumis}}{d\vec{X}},\ \underset{\text{kontroll-parameetrid}}{\alpha_i},\ \vec{X},\ t\right)$$

M - mittelineaarne funktsioon

1. $\dot{q}_1 = q_1^2 + q_1 q_2 + \ldots$ mittelinea arsus
2. $\dot{q}_1 = -\gamma q_1 + \ldots$ dissipatsi oon
3. $\dot{q}_1 = \frac{\partial q_1}{\partial X_1} + \ldots$ ruumiline muutus

   $= \frac{\partial^2 q_1}{\partial X_1^2} + \ldots$ difusioon

   $= q_1 \frac{\partial q_1}{\partial X_1} + \ldots$ konvektsio on
4. $\dot{q}_1 = \int f\left(\vec{X},\vec{X}'\right) q_1\left(\vec{X}'\right) d\vec{X}'$ mittelokaa lsus
5. $\dot{q}_1 = \alpha q_1$ α – kontrollpa rameter (juhtimine)
6. $\dot{q}_1 = c\left(\vec{X}\right) q_1$ mittehomogeensus

Näide: Iseorganiseeritus

1. Konvektsiooni mustrid
2. Minimagnetite käitumine
3. Liblikate tiivamustrid
4. Õiesüdamikud
5. M. Escheri transformatsioonid

Viited:

1. P. Ball The self-made tapestry. Pattern formation in nature. Oxford University Press, Oxford, 1999

1. Konvektsiooni mustrid

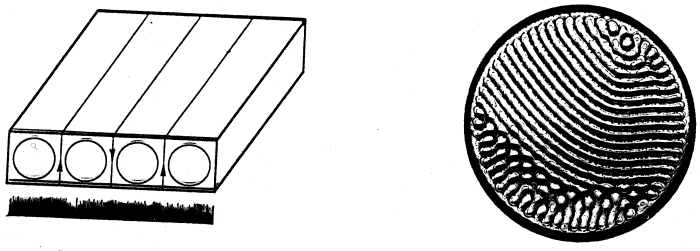

Fig. 2: Schematic drawing of the Bénard experiment and a typical flow pattern.

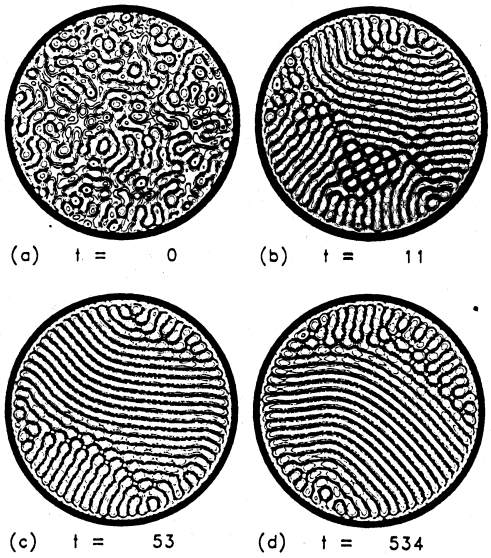

Fig. 9: The emergence of convective patterns in the Bénard experiment. (after [20]).

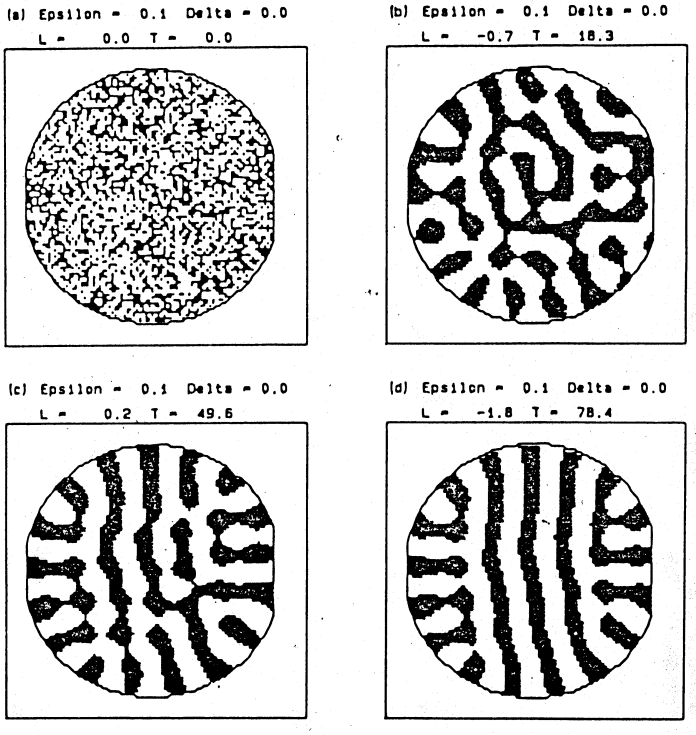

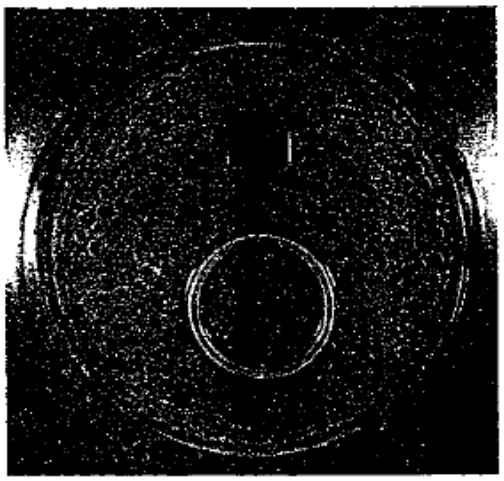

Fig. 7.2 When heated uniformly from below, a layer of fluid will develop convection cells, within which warm, less dense fluid rises and cool, denser fluid sinks. (Photo: Manuel Velarde, Universidad Complutense, Madrid.)

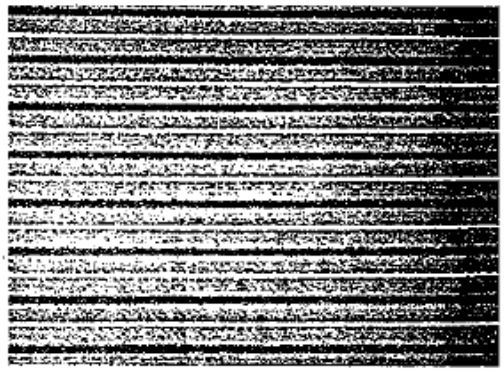

a

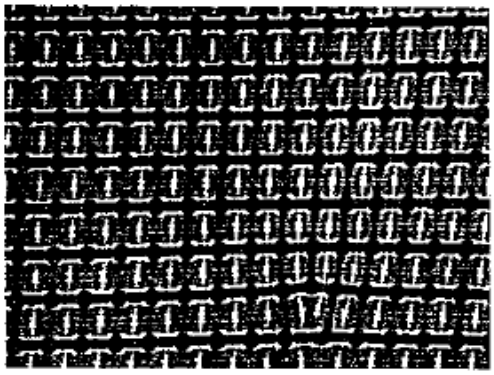

b

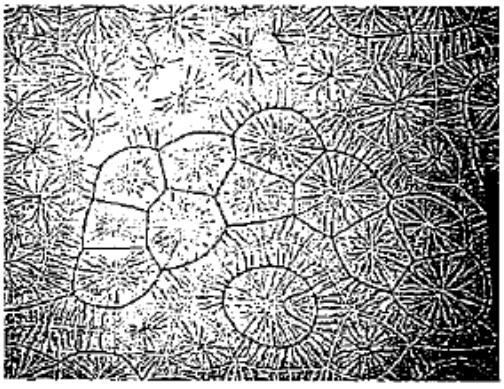

c

Fig. 7.4 The complexity of convection patterns increases as the driving force—the temperature gradient from the bottom to the top of the vessel, measured as a quantity called the Rayleigh number—is increased. The convection cells that first appear are roll cells (*a*); at higher Rayleigh numbers, rolls develop in the perpendicular direction too, and the pattern consists of roughly square cells (*b*). This is called bimodal flow. At still higher Rayleigh numbers, the pattern becomes irregular and changes with time (*c*). This 'spoke pattern' is turbulent. (From: Tritton 1988.)

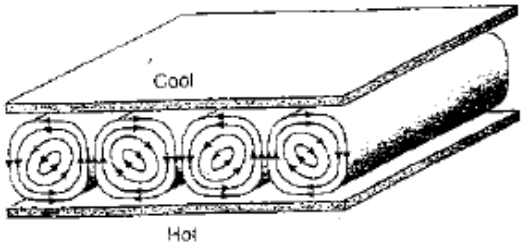

Fig. 7.3 Convection roll cells, which appear in a fluid confined between a hot bottom plate and a cooler top plate. The cells are roughly square in cross-section, and adjacent cells rotate in opposite directions.

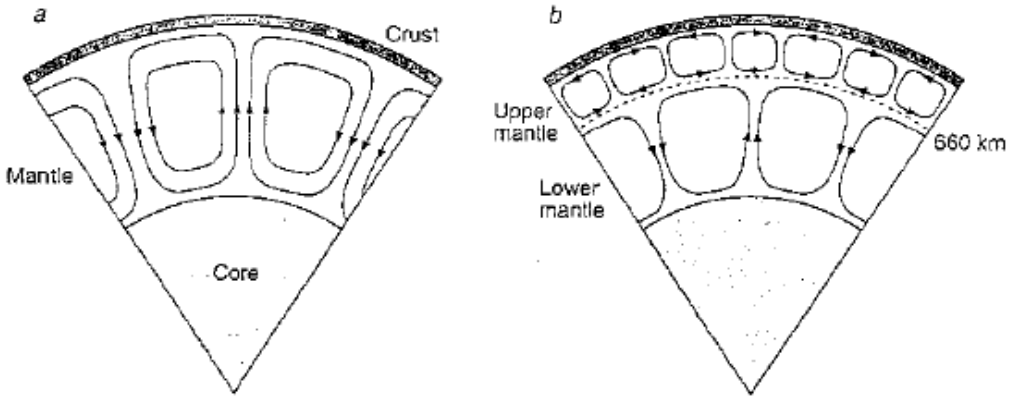

Fig. 7.16 Convection in the Earth's mantle may occur either in one layer or in two. In the former case, convection cells rotate throughout the whole mantle (*a*); in the latter, there are two layers of independent cells separated at a depth of about 660 km (*b*).

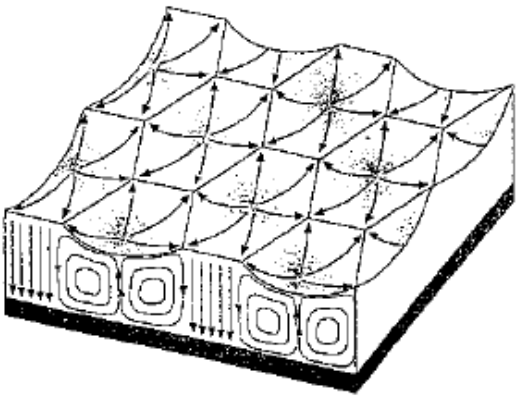

Fig. 7.15 Marangoni convection takes place in liquids that have a free top surface. Although it gives rise to hexagonal cells like those that can be seen in Rayleigh–Bénard convection (where the fluid is confined between two plates), the origin of the pattern is different. It results from imbalances in surface tension, owing to variations in temperature at the liquid surface. This causes the surface to pucker up into hexagonal cells, in which the liquid is pulled from the centre to the edges at the surface.

Mis juhtub konvektsioonis

Plate 16 Freeze-thaw cycles of groundwater at the edge of a lake in Norway produce convection cells that are traced out by stones on the lake bed. (Photo: Bill Krantz, University of Colorado.)

Fig. 7.24 The freezing and thawing of water in the soils of northern tundra sets up convective circulation owing to the unique density changes that water undergoes close to its freezing point. The imprint of this circulation can be seen as polygonal cells of stones at the ground surface. Shown here are stone polygons on the Breggerhalvoya peninsula in western Spitsbergen, Norway. (Photo: Bill Krantz, University of Colorado.)

2. Minimagnetite käitumine

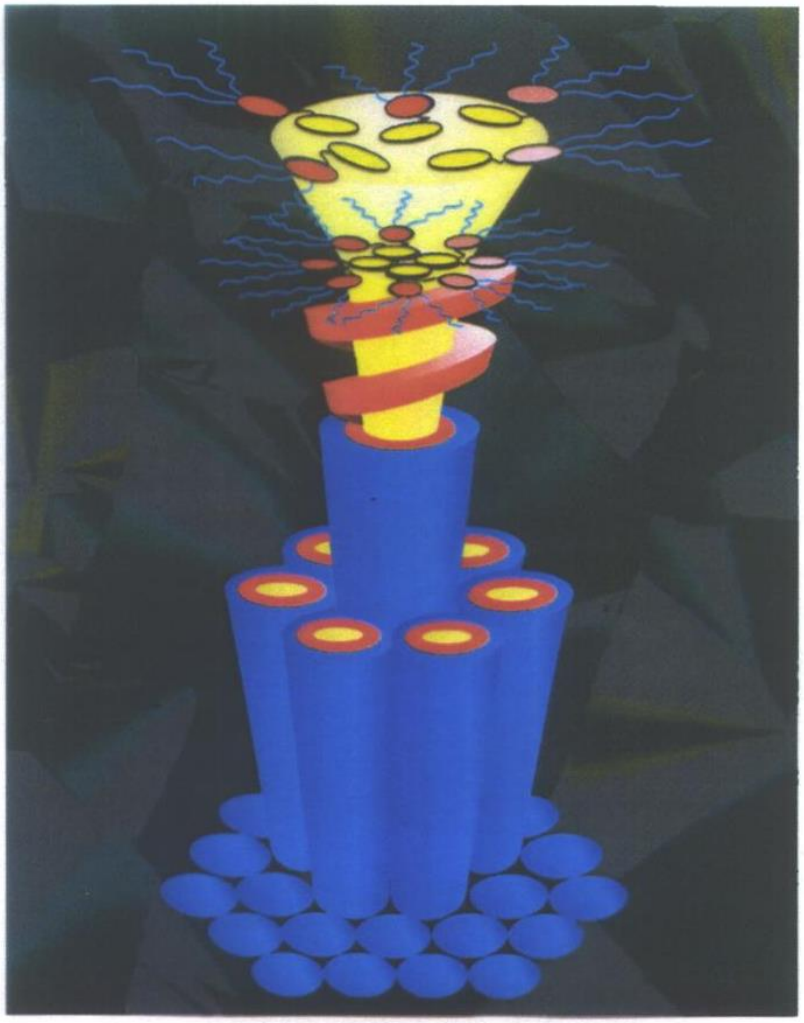

Self-organizing, cylindrical, supramolecular conglomcrate. Areas with an optoelectrical function are centrally-located. At the very top, 'pieces of cake' combine with each other to form a disc. Stacked up, these discs form a cylinder.

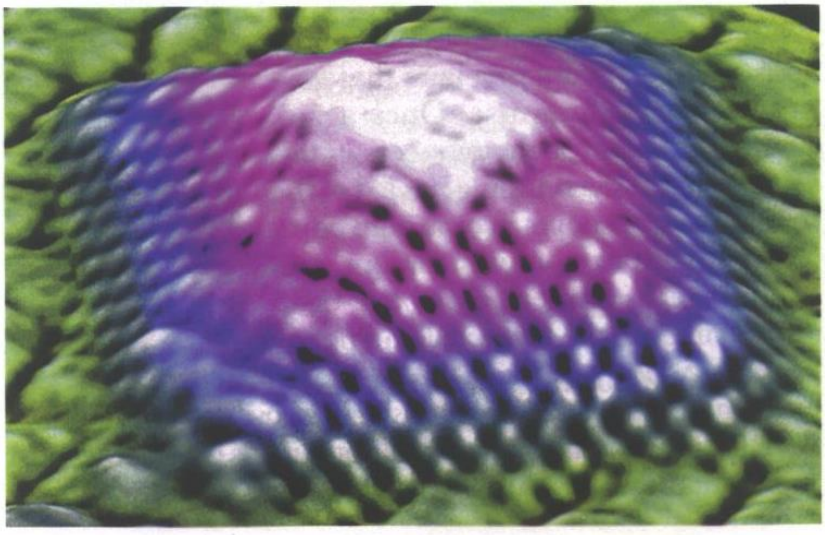

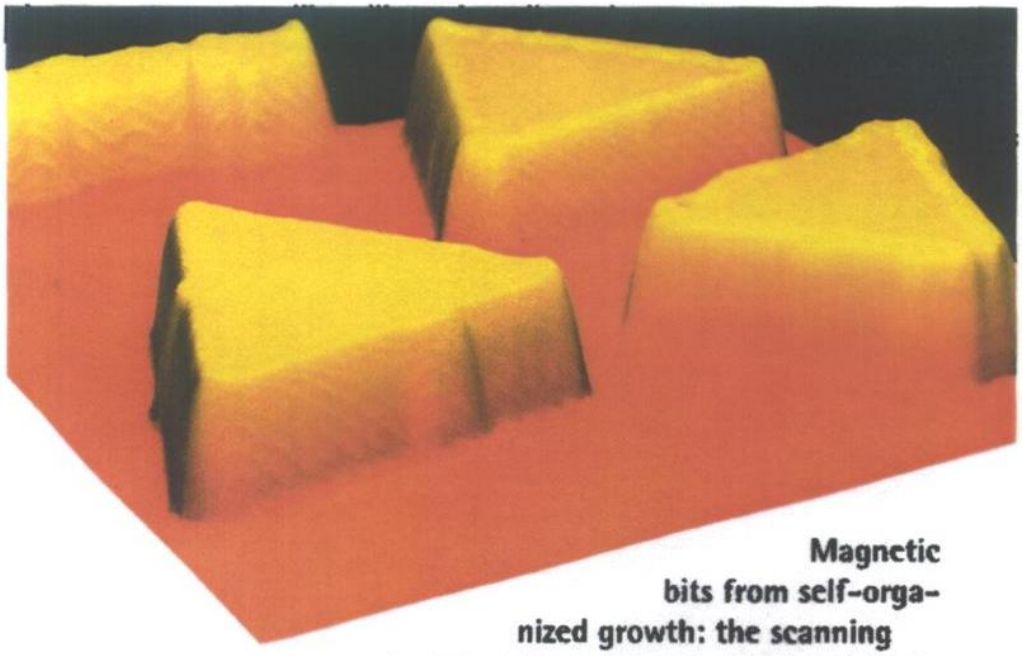

Magnetic bits from self-organized growth: the scanning electron micrograph shows cobalt islands with edges of ten nanometers in length (thousand millionth of a meter) on a copper surface. The islands contain some hundreds of atoms.

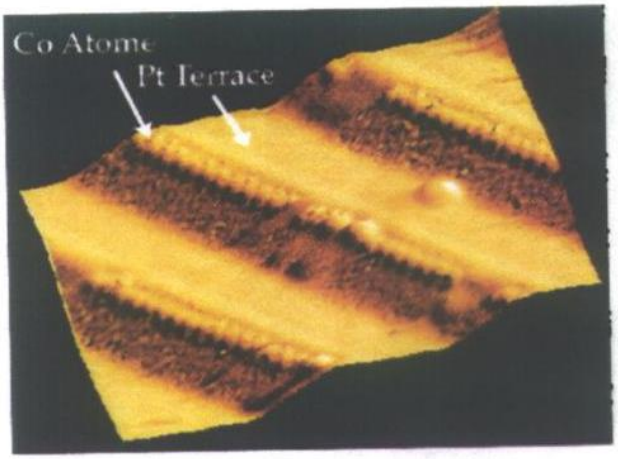

Scanning electron microscope image of chains of single cobalt atoms, lying on the steps of a platinum surface. The distance between the cobalt chains is only two nanometers.

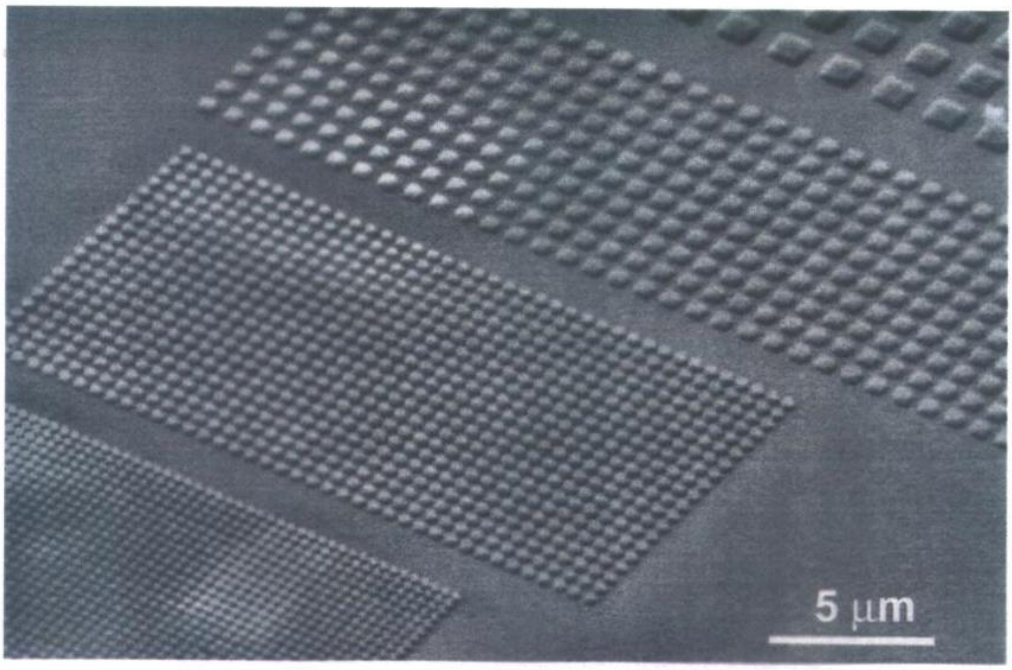

Scanning electron micrograph of ferroelectric test structures composed of lead zirconate-titanate (μm: micrometer, millionth of a meter).

The ultimate limit to miniaturization

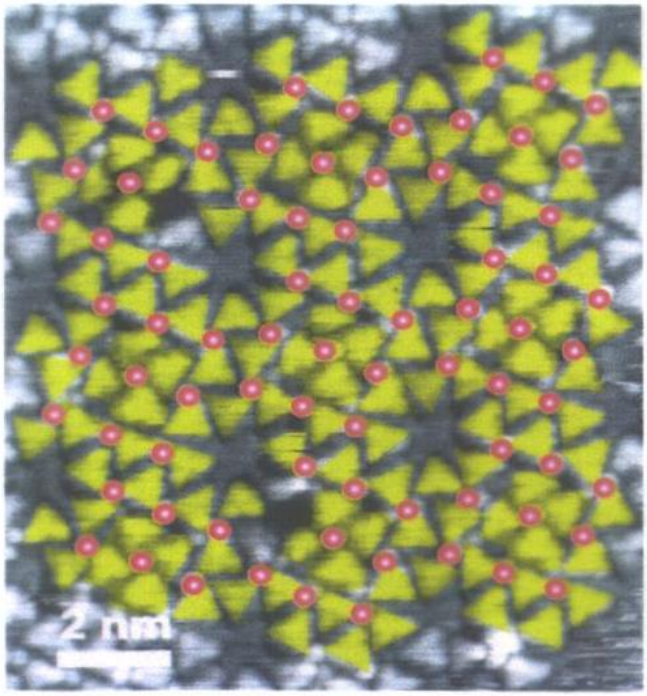

"Store" of individual magnetic iron atoms (red) in a grid formed by the spontaneous organization of organic complexes (green) on a copper surface.

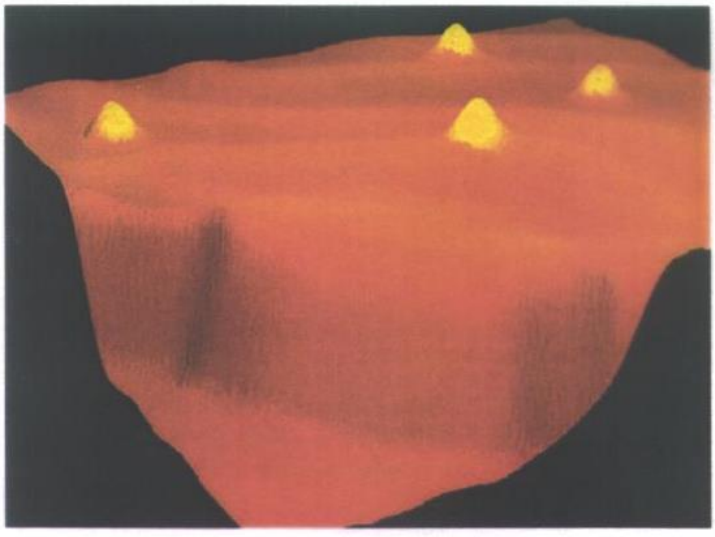

Scanning electron micrograph of four individual magnetic cobalt atoms, which were deposited on the gold surface with another technique.

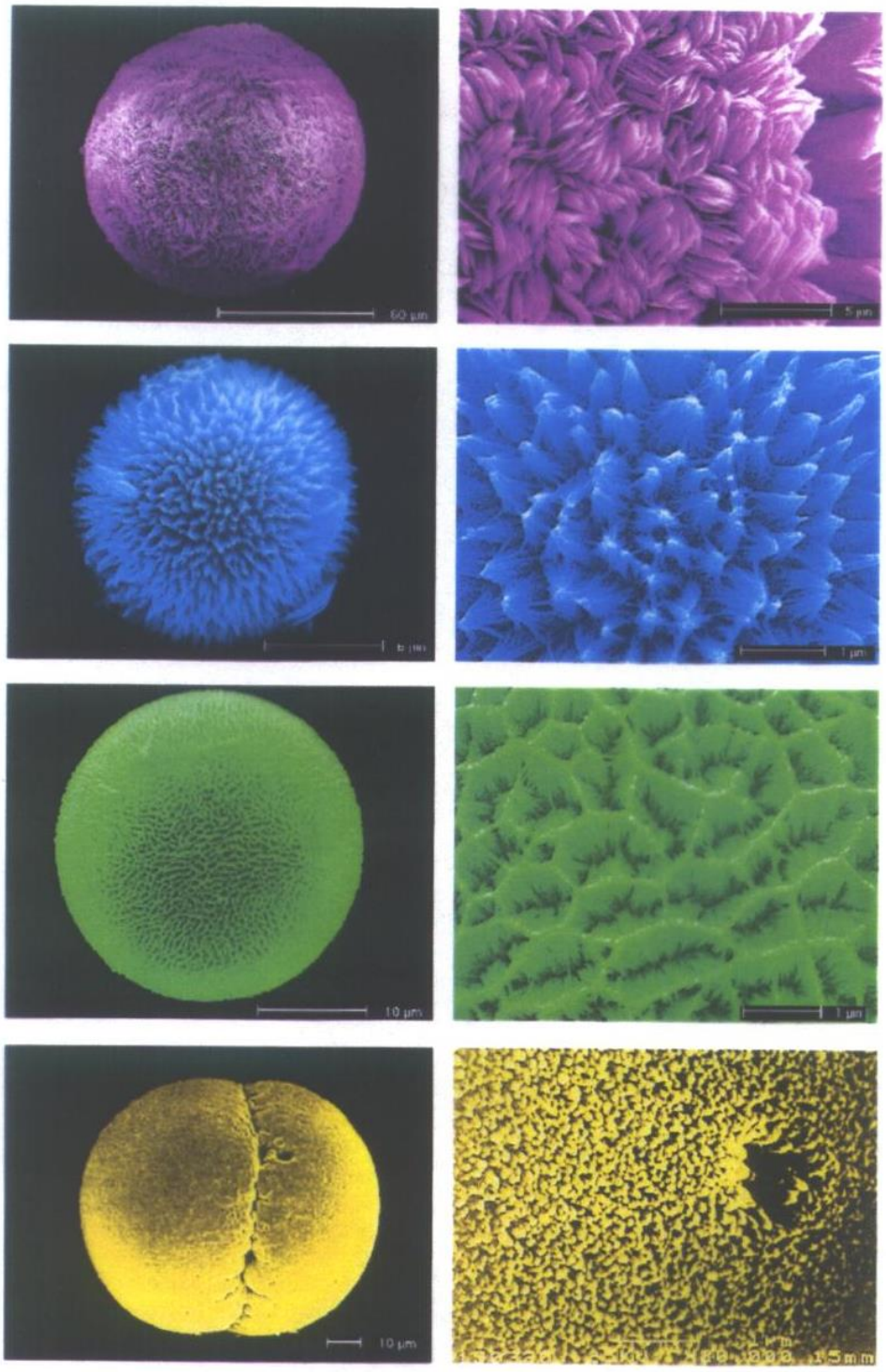

Spherical composite aggregates composed of calcium phosphate and gelatin grow via self-organization. The surface structure changes with increasing amounts of fluoride (from top to bottom); notched sphere aggregates form from fluoroapatite. (Top panel: octa-calciumphosphate, middle panel: apatite with increasing amounts of fluoride, below: fluorapatite).

3. Liblikate tiivamustrid

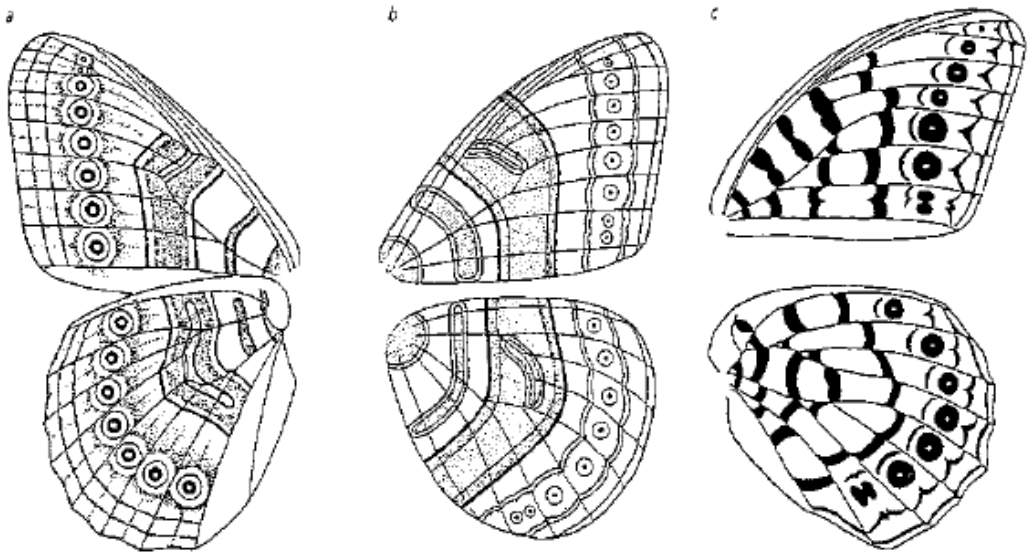

Fig. 4.25 The nymphalid ground plans of (*a*) Schwanwitsch and (*b*) Süffert represent the Platonic ideal of all butterfly and moth wing patterns. They both contain features from which almost all observed patterns can be derived. An updated version of the ground plan (*c*) takes more explicit account of the effect of wing veins. (Images: H. Frederik Nijhout, Duke University.)

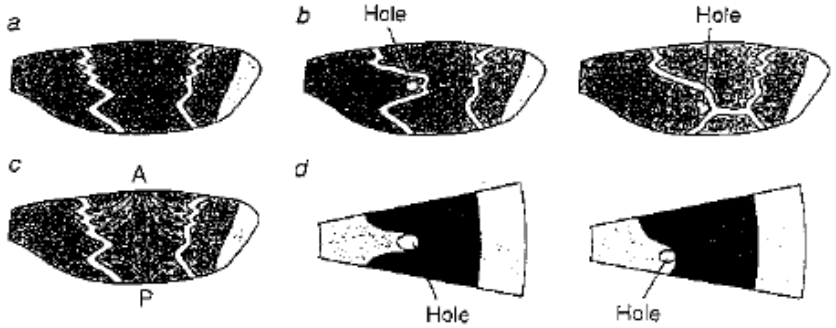

Fig. 4.28 (*a*) The moth *Ephestia kuhniella* has a central symmetry system defined by two light bands. (*b*) Kühn and von Engelhardt investigated the formation mechanism of these bands by cauterizing holes in pupal wings and observing the effect on the pattern. (*c*) They hypothesized that the disruptions of the pattern can be explained by invoking 'determination streams' of some chemical morphogen issuing from centres located on the anterior (A) and posterior (P) edges of the wing. (*d*) There is some correspondence between the pattern boundaries in these experiments and those generated in an idealized model in which a reaction–diffusion system switches on genes that fix the pattern. (After: Murray 1990.)

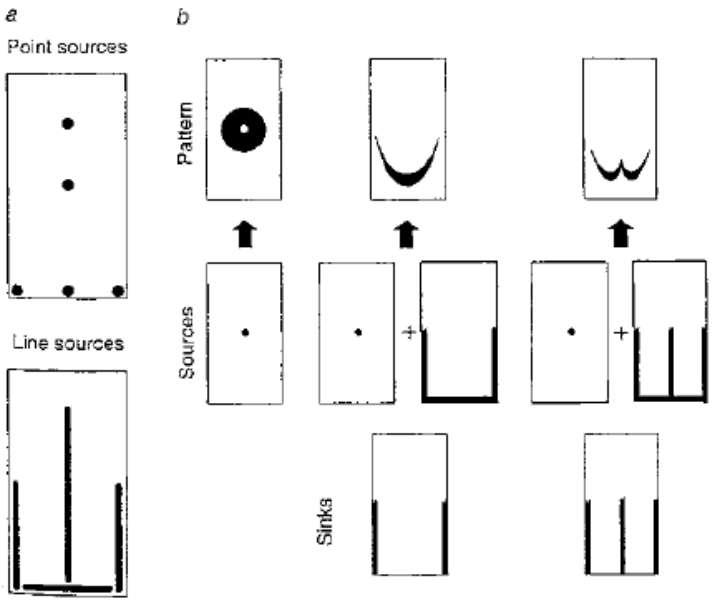

Fig. 4.29 A set of sources and sinks of morphogen (*a*) in an idealized wing cell (here shown as a rectangular unit with veins at the edges and the wing edge along the bottom) can be combined to generate many of the pattern features observed in nature (*b*). (After Nijhout 1991.)

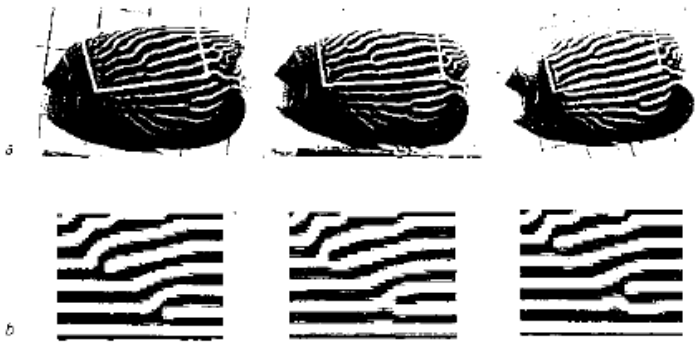

Fig. 4.24 Complex pattern reorganization in the dorsal and ventral regions of *Pomacanthus imperator* (*a*), is also captured by the model (*b*). (Photos: Shigeru Kondo.)

4. Õiesüdamikud

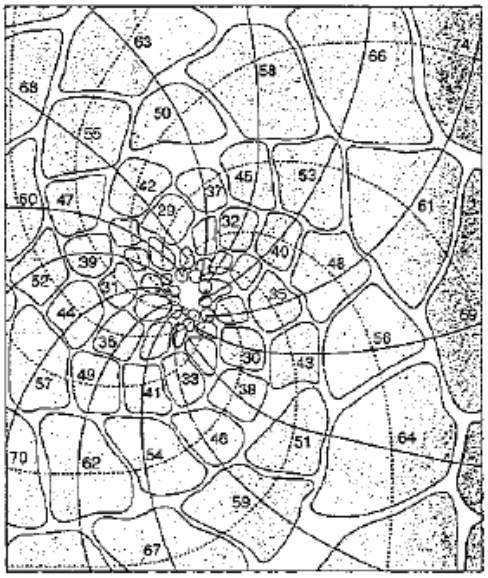

Fig. 4.39 The pattern of spiral phyllotaxis in the monkey puzzle tree. Here I show the projection of the pattern onto a two-dimensional plane, looking down the axis of the branch. Leaves are numbered consecutively from the youngest, and the two systems of spirals (solid and dashed lines) indicate leaves that are in contact with one another. (After Goodwin 1994.)

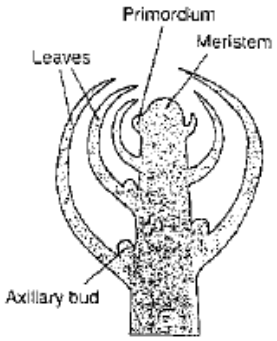

Fig. 4.38 The pattern of phyllotaxis is determined at the tip of the growing stem (the meristem), where the leaf buds (primordia) are initiated. (After Koch and Meinhardt 1994.)

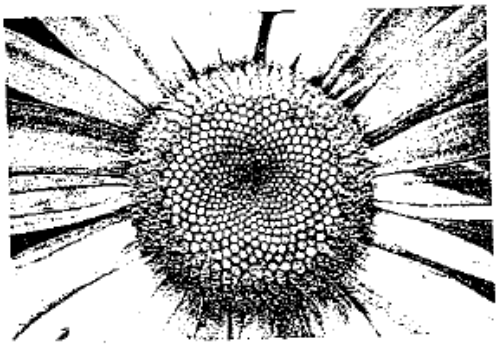

a

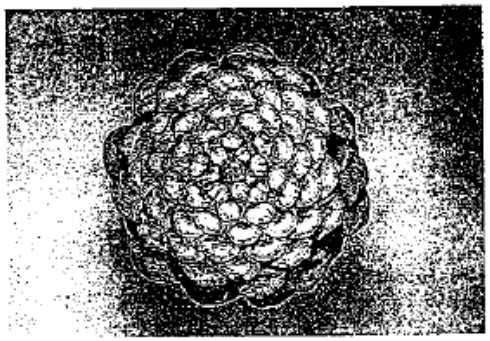

b

Fig. 4.40 The double spiral pattern of phyllotaxis is particularly clear in the arrangement of florets in a flower head (a) and of leaflets in a pine cone (b). (Photos: Scott Camazine, Pennsylvania State University.)

5. M. Escheri transformatsioonid

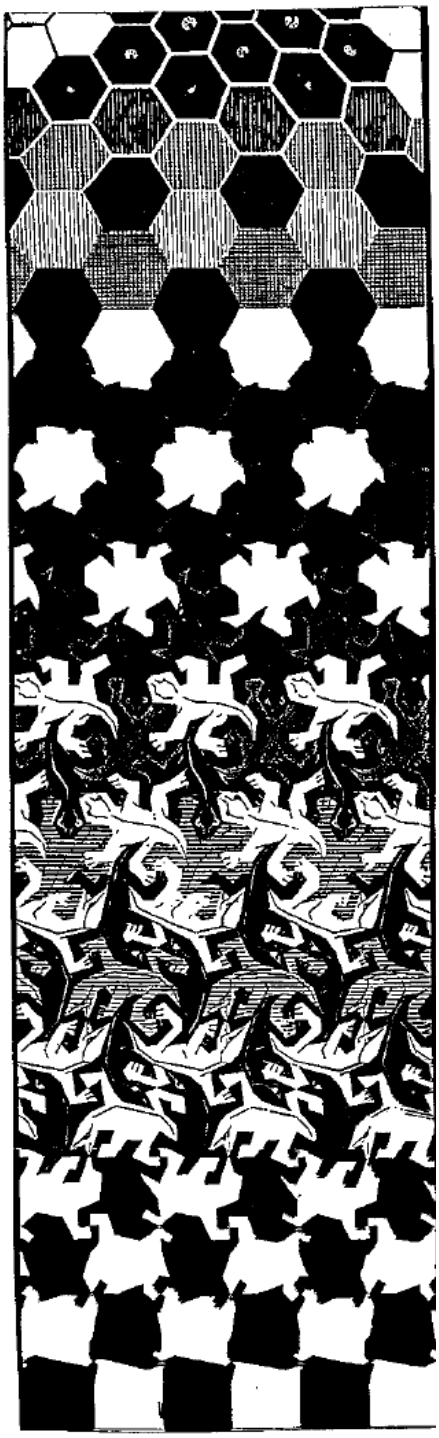

6. Galaktikad

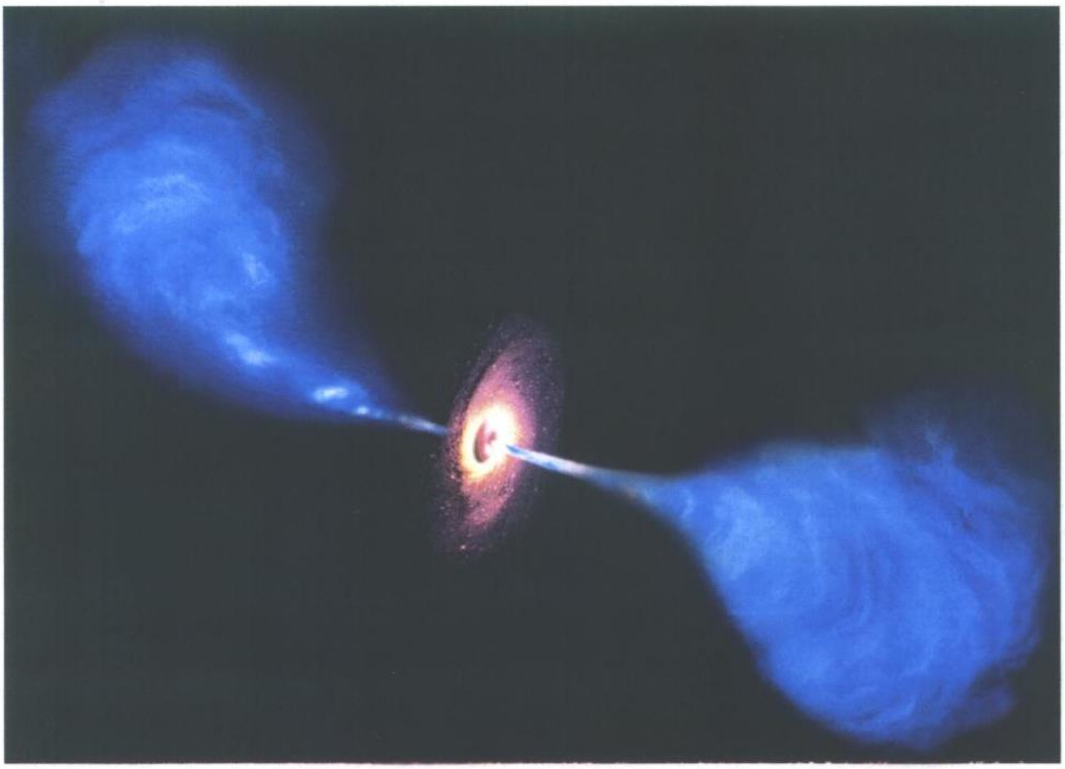

Quasars are among the most intensely radiating objects in the universe. Within a distance of only a few light years, they produce a thousand to some hundreds of thousand times more electromagnetic energy than whole star systems. Quasars lie in the centers of large galaxies and are evidently "driven" by supermassive black holes.

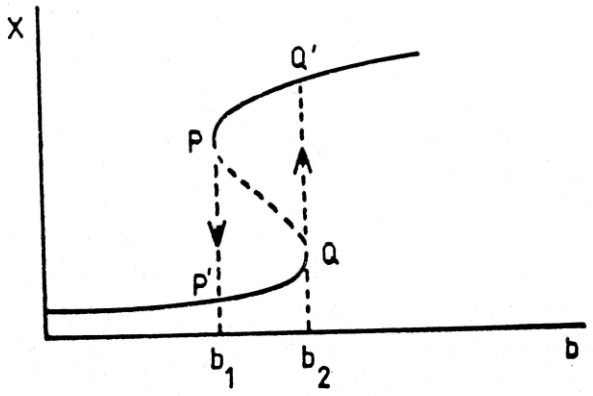
X
Q'
P
Q
P'
b1
b2
b

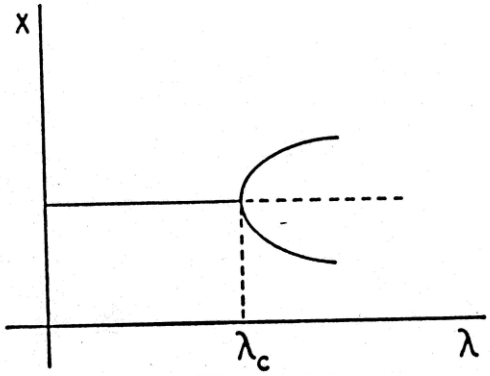
X
λc
λ

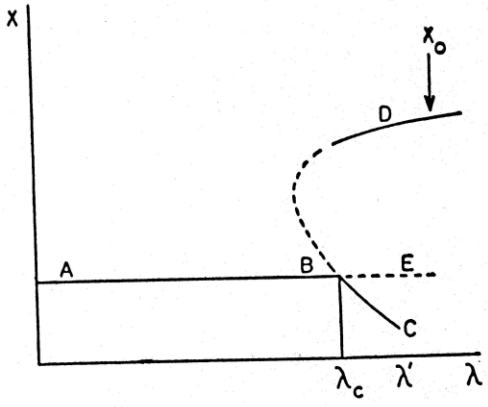
X
Xo
D
A
B
E
C
λc
λ'
λ

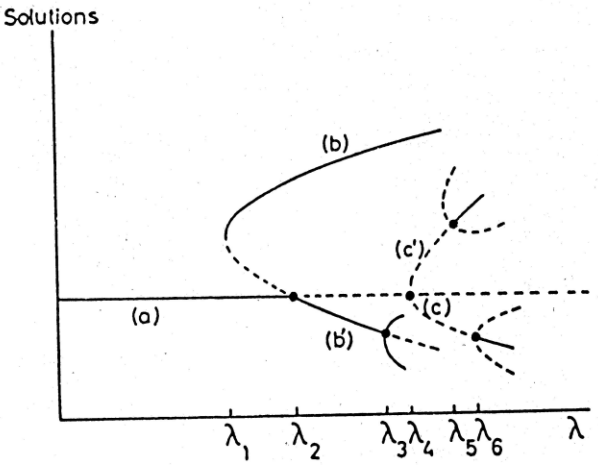
Solutions
(b)
(c')
(c)
(a)
(b')
λ1
λ2
λ3
λ4
λ5
λ6
λ

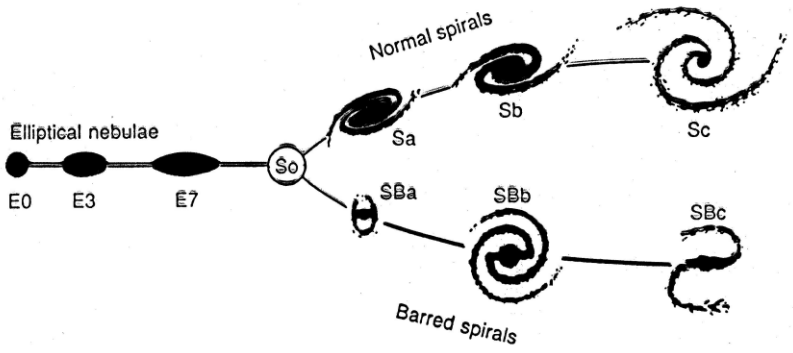

Figure 6.6 Hubble's picture of his sequence

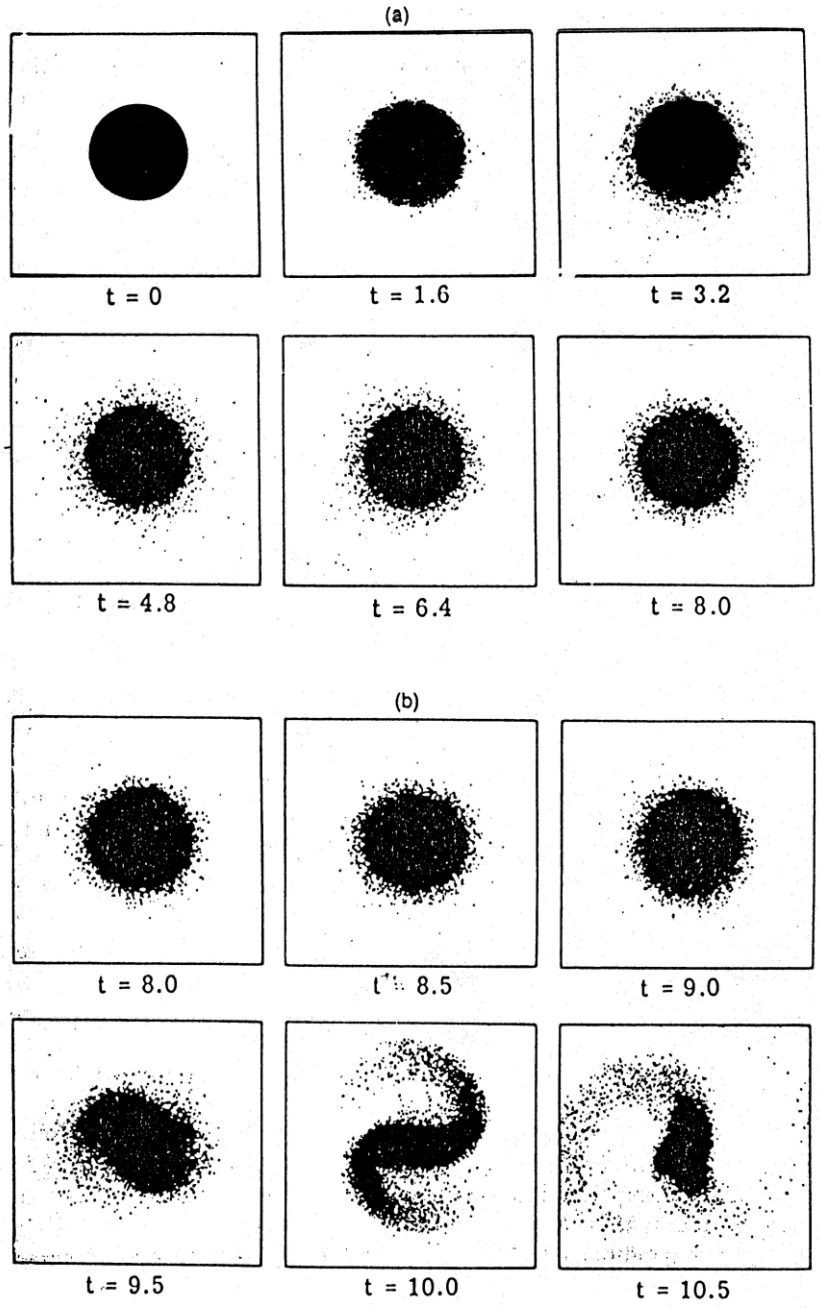

Figure 6.7 Computer simulation of the dynamics of a circular disc of stars. (a) Requiring symmetry to be preserved. (b) Allowing it to break

Näide: Liivakuhikud ja liivadüünid

1. Düünid looduses
2. Lihtne liivakuhiku mudel
3. Täpsustatud liivakuhiku mudel
4. Osakeste kuju mõjutab varinguid

1. Düünid looduses

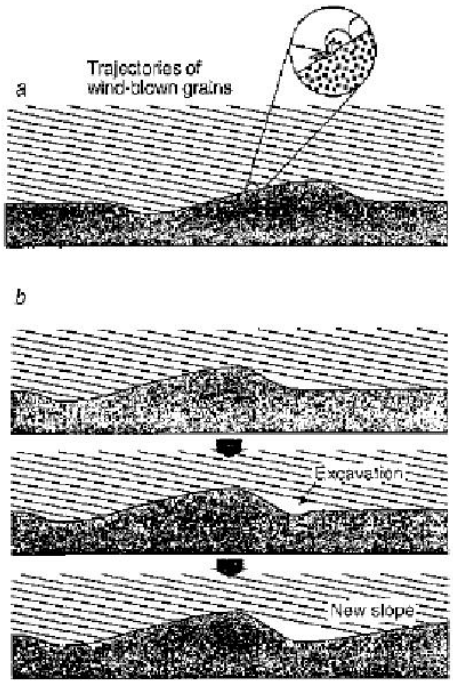

Fig. 8.23 The formation of sand ripples involves a propagating instability. Wind-borne sand grains rain down on the desert surface at an oblique angle. Where the surface slopes, more grains impact the windward (stoss) side of the slope than the leeward side (*a*). Each grain scatters others from the surface as it strikes, and travels in the downwind direction for a few short hops (a process called saltation) before coming to rest. The accumulation of saltating grains at the slope crest means that the leeward foot of the slope receives fewer new grains than other regions, and so it begins to be excavated into a depression (*b*). This depression develops into a new, downwind stoss slope, and a new ripple is formed.

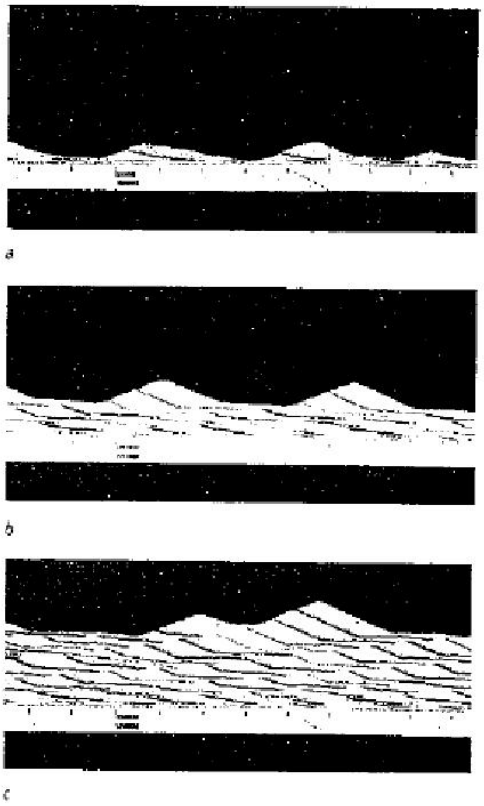

Fig. 8.24 Self-organized ripples appear in a cellular-automaton model of wind-blown sand deposition. The ripples develop on a flat surface as the growth instability amplifies small irregularities (*a*). These ripples move from left to right owing to saltation. Because of the difference in speed between smaller, faster ripples and larger, slower ones, they exchange mass until their size, speed and spacing is more or less uniform (*b*). 'Stained' grains injected at regular intervals reveal the patterns of layer deposition for different deposition rates (*b*, *c*). (Images: Peter Hoff, Duke University, North Carolina. Reproduced from Forrest and Hall (1992). *Science* 255, 1240.)

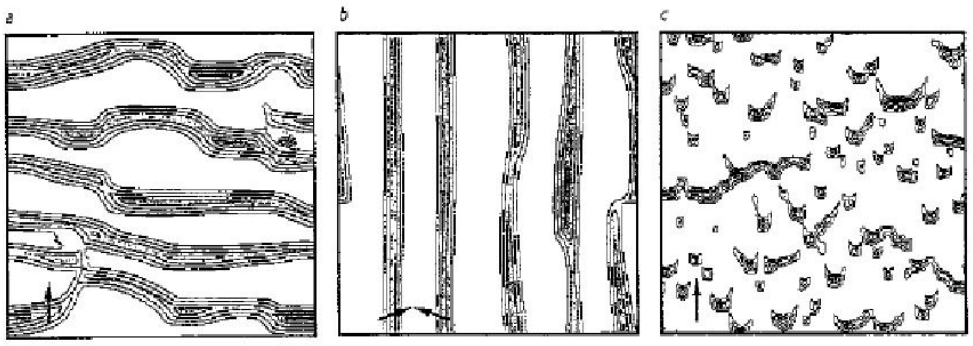

Fig 8.25 A cellular–automaton model of dune formation generates many of the major dune types, including transverse and longitudinal ripple dunes (*a*, *b*) and barchan dunes (*c*). Here I show the contours of the deposited material. The shapes depend on the wind direction and variability (indicated by arrows). (Images: from B.T. Werner (1995). *Geology* 23, 1107.)

Plate 23 Sand dunes are an example of a self-organized pattern on a grand scale. (Photo: Jackie Cohen.)

a

b

Fig. 8.25 Large-scale sand transport can create dunes of several characteristic shapes, including the crescent-shaped barchan dunes (*a*) and the many-armed star dunes (*b*). (Photos: Nick Lancaster, Desert Research Institute, Nevada.)

A

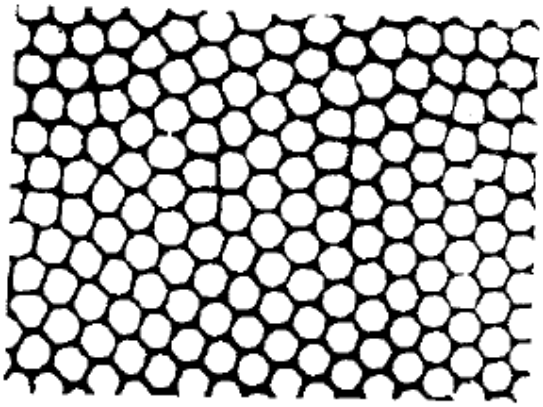

B

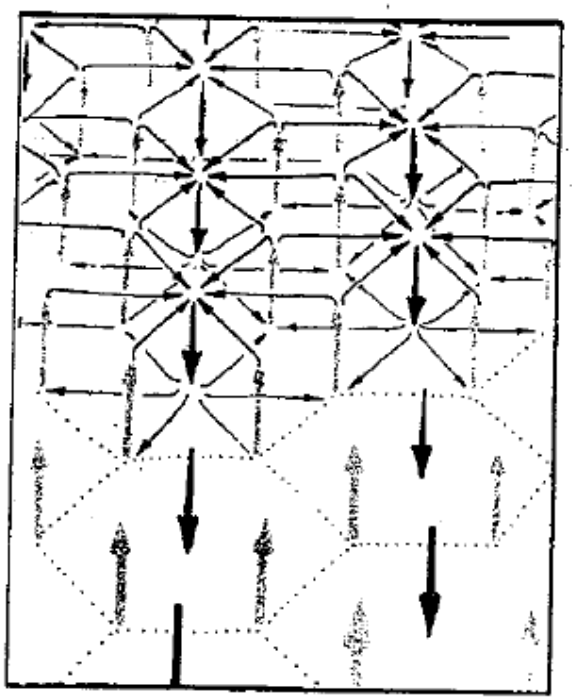

C

2. Lihtne liivakuhiku mudel

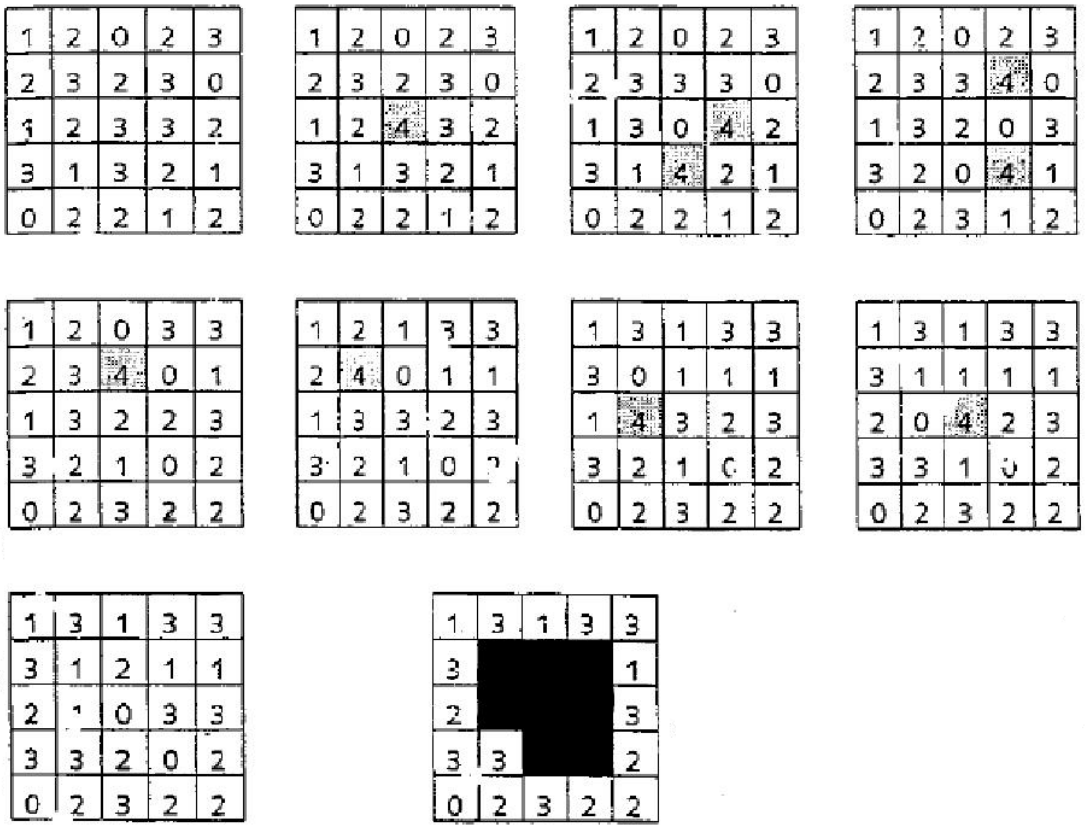

Figure 12. Illustration of toppling avalanche in a small sandpile. A grain falling at the site with height 3 at the center of the grid leads to an avalanche composed of nine toppling events, with a duration of seven update steps. The avalanche has a size $s = 9$. The black squares indicate the eight sites that toppled. One site toppled twice.

$$Z(x,y) \to Z(x,y)+1$$
$$Z(x,y) \to Z(x,y)-4$$
$$Z(x\pm1,y) \to Z(x\pm1,y)+1$$
$$Z(x,y\pm1) \to Z(x,y\pm1)+1$$

3. Täpsustatud liivakuhiku mudel

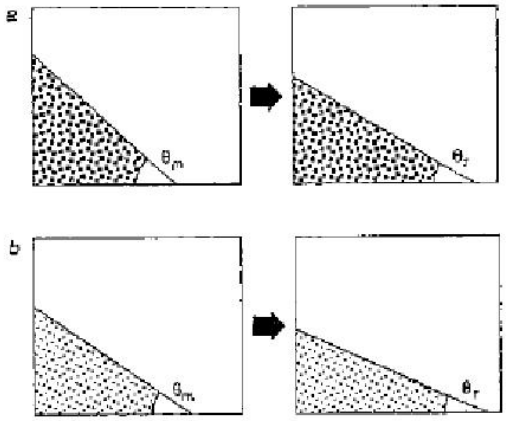

Fig. 8.10 A pile of grains will undergo an avalanche at a critical angle θ_m, the angle of maximum stability. The avalanche will cause the slope to 'relax' to a stable angle θ_r, the angle of repose. These angles will generally differ for grains of different shapes.

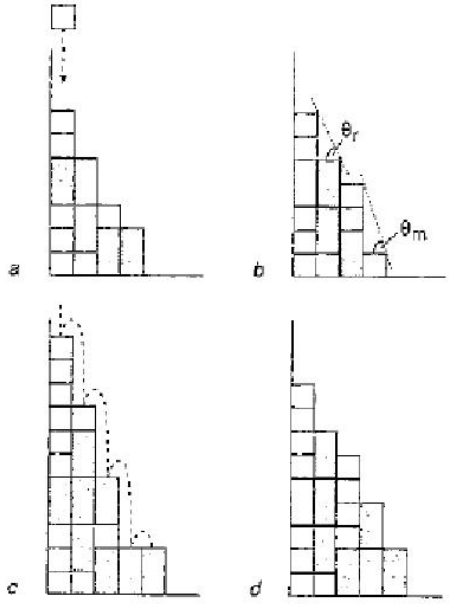

Fig. 8.11 The stratification that takes place when mixed grains are poured can be mimicked in a simple theoretical model in which the two grains have different shapes: square and rectangular. The model assumes that as they are poured, the grains stack up into columns, with all of the rectangular grains upright (a). Although this is a highly artificial assumption, it reproduces the effect of different grain shapes, which is the cause of the stratification. The angle of maximum stability θ_m is such that the difference in height between one column and the next cannot exceed three times the width of the square grains, and the angle of repose θ_r is equivalent to a height difference of two (b). If a new grain added to the top of the slope creates a slope greater than θ_m, it tumbles from column to column until it finds a stable position (c). But if the grain has to go all the way to the foot of the pile (as in c), this implies that the slope is equal to θ_m everywhere. The pile then undergoes a landslide to reduce the slope everywhere to θ_r or less (d). (After Makse *et al.* 1997.)

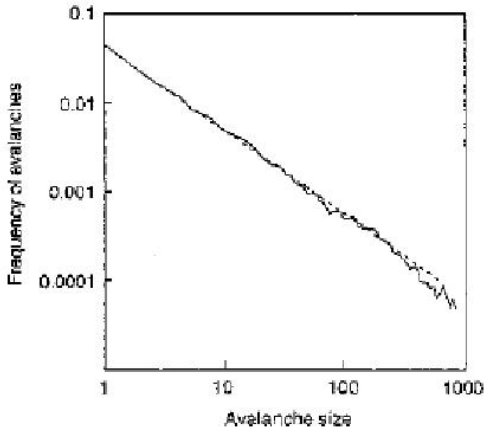

Fig. 8.17 The frequency of an avalanche of a certain size (that is, involving a certain number of grains) decreases in inverse proportion to its size. In a simple model of sand-pile avalanches. On a plot of the logarithm of frequency against the logarithm of size, this relationship defines an approximately straight line with a slope of around minus one (depicted by the dashed line). (After Bak 1997.)

4. Osakeste kuju mõjutab varinguid

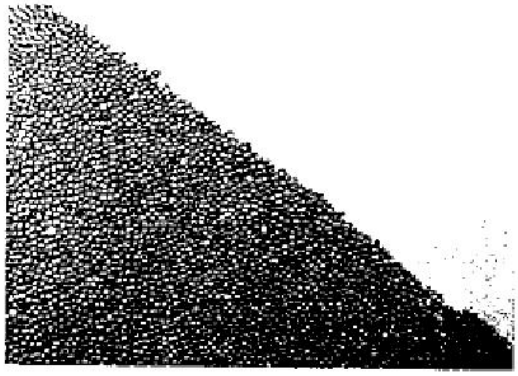

a

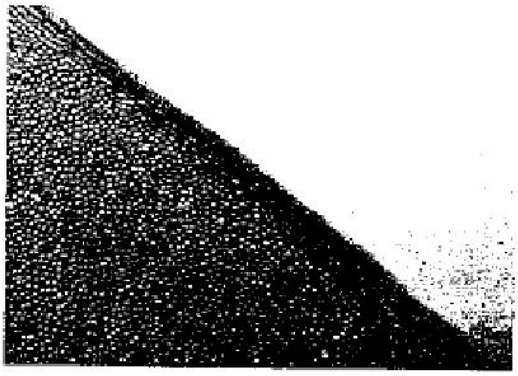

b

Fig. 8.16 The slope of a granular heap varies locally from place to place (a). In this pile of mustard seeds, small variations in slope can be seen superimposed on a constant average gradient. When the slope approaches the angle of maximum stability, the addition of a single seed can trigger an avalanche (b). This avalanche can involve any number of grains, from just a few to the entire slope. Notice that only grains within the first few layers move (there the grains in motion are blurred). (Photos: Sidney Nagel, University of Chicago).

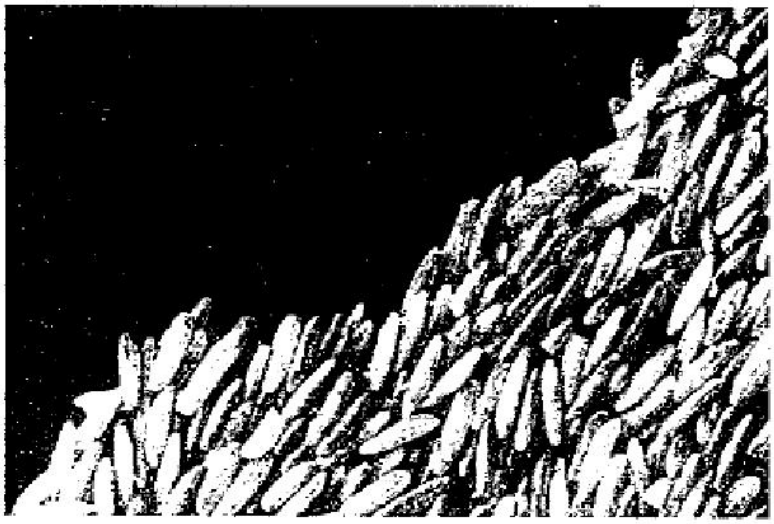

Fig. 8.21 A section of a rice pile confined between two glass plates. Notice how uneven the slope is on this fine scale. (Photo: Kim Christensen, University of Oslo.)

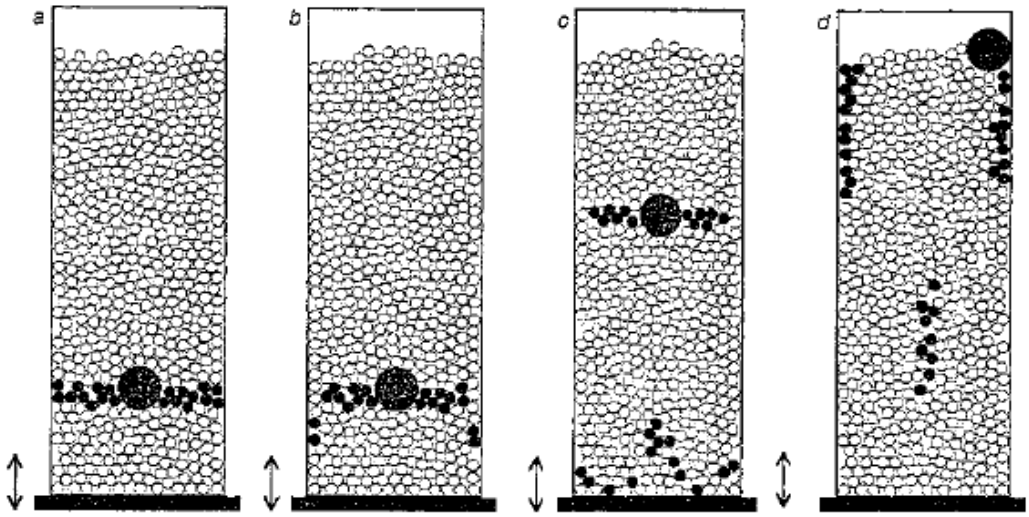

Fig. 8.2 Grains in a tall column undergo convection-like circulating motions: the grains in the centre rise upwards, and those at the edges crawl down to the bottom in a narrow band. The images shown here are reconstructions of an experiment in which some glass beads were dyed to reveal their motions. An initially flat layer near the bottom of the column (*a*) separates into down-going beads at the edges and rising beads at the centre (*b*). The latter move outwards at the top and then downwards at the walls (*d*); the former move upwards at the centre when they reach the bottom (*c*, *d*). A single large bead gets trapped at the top because it is too large to fit in the narrow down-welling band at the edges. So the convective motion causes size segregation. (Images: Sidney Nagel, University of Chicago.)